THE ASTROPHYSICAL JOURNAL, 375:177–189, 1991 July 1

A SIMULATION OF THE COLLAPSE AND FRAGMENTATION OF COOLING MOLECULAR CLOUDS

JOE J. MONAGHAN
Department of Mathematics, Monash University, Clayton, Victoria, 3168, Australia

AND

JOHN C. LATTANZIO
Institute of Geophysics and Planetary Physics, Lawrence Livermore National Laboratory, L-413, P.O. Box 808, Livermore, CA 94550; and Astronomy Department, University of California, Berkeley
Received 1989 December 4; accepted 1990 December 10

ABSTRACT

We describe the application of the Smoothed Particle Hydrodynamics method to the fragmentation of rotating cloud and disk systems, allowing for molecular cooling due to H_2 and CO. We also describe a novel approach to solving Poisson's equation for disklike structures, which exploits the multigrid algorithm. Numerical studies are presented which investigate the evolution of both rotating clouds and Maclaurin disks, in each case with both an isothermal equation of state and with molecular cooling. Our results establish the influence of molecular cooling on the fragmentation of molecular clouds. The isothermal sequences, if they fragment at all, do so into far fewer lumps than the cooling sequences. This is not due to a cooling instability as such, but rather to the reduced thermal support. One of our sequences shows a remarkable similarity to the W49A star-forming region.

Subject headings: hydrodynamics — interstellar: molecules — nebulae: individual (W49) — nebulae: structure

1. INTRODUCTION

It is generally believed that large clouds of molecular gas fragment and produce stars. However, the details of this mechanism are unknown. In the absence of reliable information about the structure of these clouds it is reasonable to examine simple geometries such as spheres, disks, cylinders etc., in order to gain some insight into the fragmentation process (see Larson 1985 for a review). The calculations are usually further simplified by the assumption of an isothermal equation of state. This last assumption is, however, unnecessarily crude since molecular gas is expected to cool rapidly and appropriate cooling functions are known.

In this paper we describe a Smoothed Particle Hydrodynamics (SPH) program which incorporates the cooling from H_2 and CO molecules in the optically thin approximation. In addition, substantial improvements to our multigrid algorithm for determining the gravitational field allow us to follow the evolution of clouds through to disk systems with high accuracy.

The applications we describe include the evolution of rotating clouds with and without substantial random perturbations, and with and without molecular cooling. We also study disk structures both with and without cooling. While our calculations are extensive and give a clear picture of the changes induced by molecular cooling, they do not, nor are they intended to, give a comprehensive description of star formation. Although the structures we consider here are only primitive models of real clouds, they provide us with a convenient numerical laboratory to investigate fragmentation. The calculations described here illustrate the flexibility of the computing techniques which we plan to apply to the simulation of an entire molecular cloud complex.

2. EQUATIONS OF MOTION

We use the particle method SPH (for a review see Monaghan 1988). The momentum equation

$$\frac{d\boldsymbol{v}}{dt} = -\frac{1}{\rho}\nabla P - \nabla\phi\,, \tag{2.1}$$

becomes

$$\frac{d\boldsymbol{v}_i}{dt} = -\sum_{j=1}^{N} m_j\left(\frac{P_i}{\rho_i^2} + \frac{P_j}{\rho_j^2} + \Pi_{ij}\right)\nabla_i W_{ij} - (\nabla\phi)_i\,, \tag{2.2}$$

where particle j at position $\boldsymbol{r}_j$ carries mass m_j, velocity $\boldsymbol{v}_j$ and thermal energy per unit mass u_j, and j runs from 1 to N, the total number of particles in the calculation (henceforth all sums, unless explicitly stated, extend from 1 to N). The density ρ_j at the position of particle j is given by

$$\rho_j = \sum_k m_k W_{kj}\,, \tag{2.3}$$

and the pressure P_j is obtained from the equation of state using ρ_j and the temperature T_j at r_j. The function $W_{ij} \equiv W(|\boldsymbol{r}_i - \boldsymbol{r}_j|, h)$ is the interpolating kernel. We use the spline-based kernel with compact support (Monaghan & Lattanzio 1985) which is defined by

$$h^3 W(v,h) = \begin{cases} \dfrac{3}{2\pi}\left(\dfrac{2}{3} - v^2 + \dfrac{1}{2}v^3\right); & 0 < v < 1 \\ \dfrac{1}{4\pi}(2-v)^3\,; & 1 \le v \le 2 \end{cases}$$

where $v = r/h$.

In equation (2.2) $\nabla_i W_{ij}$ denotes the gradient of W_{ij} taken with respect to the coordinates r_i. Artificial viscosity is provided by Π_{ij} which has the form

$$\Pi_{ij} = \frac{1}{\bar{\rho}_{ij}} (-\alpha \mu_{ij} \bar{c}_{ij} + \beta \mu_{ij}^2) \tag{2.4}$$

where the notation $\bar{A}_{ij} = \frac{1}{2}(A_i + A_j)$ has been used, c is the speed of sound and

$$\mu_{ij} = \begin{cases} \dfrac{h \boldsymbol{v}_{ij} \cdot \boldsymbol{r}_{ij}}{r_{ij}^2 + \eta^2}; & \text{if} \quad \boldsymbol{v}_{ij} \cdot \boldsymbol{r}_{ij} < 0 \\ 0; & \text{otherwise} . \end{cases} \tag{2.5}$$

where the notation $\boldsymbol{a}_{ij} = (\boldsymbol{a}_i - \boldsymbol{a}_j)$ has been used and $\eta^2 = 0.01h^2$ prevents the denominator from vanishing. Π_{ij} produces both a bulk and a shear viscosity. The gravitational force at particle i is denoted by $(\nabla\phi)_i$. The thermal energy equation with cooling function Λ is

$$\frac{du}{dt} = -\frac{P}{\rho} \nabla \cdot \boldsymbol{v} - \frac{\Lambda}{\rho} , \tag{2.6}$$

where u is the thermal energy per unit mass. This becomes

$$\frac{du_i}{dt} = \frac{1}{2} \sum_j m_j \left(\frac{P_i}{\rho_i^2} + \frac{P_j}{\rho_j^2} + \Pi_{ij} \right) \boldsymbol{v}_{ij} \cdot \nabla_i W_{ij} - \frac{\Lambda_i}{\rho_i} . \tag{2.7}$$

To deal with the "wall heating" effect in high speed colliding flows we add to equation (2.6) a thermal conduction term

$$\frac{1}{\rho} \nabla \cdot (\rho q \nabla u) \tag{2.8}$$

which can be approximated by

$$\sum_j m_j \frac{(q_i + q_j)(u_i - u_j) \boldsymbol{r}_{ij} \cdot \nabla_i W_{ij}}{\bar{\rho}_{ij} (r_{ij}^2 + \eta^2)} . \tag{2.9}$$

To see that this term is valid, convert the sum to an integral and Taylor expand all terms except W_{ij} about the point $\boldsymbol{r}_{ij}$. The expression (2.9) conserves thermal energy and increases the entropy. We base the thermal conductivity function q on a natural length and time scale and write

$$q_i + q_j = gh(\bar{c}_{ij} - 4\mu_{ij}) , \tag{2.10}$$

where the term involving μ_{ij} was guessed from the similar expressions devised by Noh (1987) for gas dynamic problems. We take $g = 0.25$ which gives good results for shock tube collision flows, although impacts at very high Mach number ($\gtrsim 10$) require $g = 0.5$.

3. THERMODYNAMICS

We assume the gas is composed of He and H with mass fractions $Y = 0.25$ and $X = 0.75$, respectively. The cooling formula (see § 4) assumes the gas contains small quantities of CO, but this has a negligible effect on the thermal energy. Assuming the gas is unionized (for the temperatures reached in our simulations this is true) the thermal energy per unit mass is

$$u(T) = \Re_0 T \left(\frac{3}{2} Xy + \frac{3}{8} Y \right) + \frac{1}{2} Xy \frac{D_0}{m_H} + \frac{X(1-y)E(H_2)}{2m_H} , \tag{3.1}$$

where m_H is the mass of an H atom, D_0 is the dissociation energy of H_2 (4.477 eV), y determines the number of H atoms (see below), and $E(H_2)$ is the energy of an H_2 molecule.

The parameter y is defined by

$$y = \frac{\rho(H)}{\rho X} , \tag{3.2}$$

where $\rho(H)$ is the mass density of atomic H and ρ is the mass density of the gas. Thus

$$\rho X = \rho(H) + \rho(H_2) , \tag{3.3}$$

where $\rho(H_2)$ is the mass density of H_2. From equilibrium theory

$$\frac{y^2}{1-y} = \frac{2.11}{\rho X} e^{-52490/T} , \tag{3.4}$$

which fits the values given by Aller (1964, p. 119) to within a few percent.

The energy of the H_2 molecule is given by

$$E(H_2) = \tfrac{3}{2}kT + \text{rotation} + \text{vibration} . \tag{3.5}$$

We take the rotation temperature $\theta_{rot} = 85.4$ K and the vibration temperature θ_{vib} to be 6100 K. From the para–partition function

$$z_p = \sum_{j=0,2,4,\ldots}^{\infty} (2j+1) e^{-j(j+1)\theta_{rot}/T} \tag{3.6}$$

and the ortho–partition function

$$z_o = \sum_{j=1,3,5,\ldots}^{\infty} (2j+1) e^{-j(j+1)\theta_{rot}/T} , \tag{3.7}$$

we calculate

$$f_p = T^2 \frac{\partial \ln z_p}{\partial T} , \quad f_0 = T^2 \frac{\partial \ln z_o}{\partial T} . \tag{3.8}$$

The rotational energy is then kf_{tot} where (assuming statistical equilibrium)

$$f_{tot} = \frac{z_p f_p + 3 z_o f_o}{z_p + 3 z_o} . \tag{3.9}$$

Finally

$$E(H_2) = k \left[\frac{3}{2} T + f_{tot} + \frac{\theta_{vib}}{\exp(\theta_{vib}/T) - 1} \right] . \tag{3.10}$$

The equation of state is

$$P = \frac{\rho \Re_0 T}{\mu} , \tag{3.11}$$

where the temperature is obtained from equation (3.1) and

$$\frac{1}{\mu} = \left[\frac{X}{2} (1 + y) + \frac{Y}{4} \right] . \tag{3.12}$$

Each of our SPH particles therefore represents a piece of fluid containing, in general, H, H_2 and He (with trace amounts of CO).

4. COOLING FUNCTION

The cooling function is based on the work of Hollenbach & McKee (1979, hereafter HM) which allows us to include cooling from CO, CH, H_2O, HCl, and H_2. In the calculations which follow CO and H_2 provide the cooling. The other molecules were not included because we do not have reliable esti-

mates of their number density. A good review of heating and cooling in molecular clouds is given by Hollenbach (1988). We have included a cosmic-ray heating term (Hollenbach 1988), but its influence is tiny. Substantial heating is mainly due to radiation from nearby stars, but the inclusion of this source would be inappropriate for our calculations.

The cooling function is complicated, and our description of it is intended merely to provide a guide to the relevant parts of HM.

Let $n(\mathrm{H})$ be the number density of atomic hydrogen, and $n(\mathrm{H}_2)$ the number density of molecular hydrogen; thus $n_{\rm tot} = n(\mathrm{H}) + 2n(\mathrm{H}_2)$ is the number density of H atoms in all forms. We write Λ (ergs cm^{-3} s^{-1}) in the form

$$\Lambda = 8.5 \times 10^{-5} n_{\rm tot}^2 L(\mathrm{CO}) + n(\mathrm{H}_2)^2 L(\mathrm{H}_2) + n(\mathrm{H}) n(\mathrm{H}_2) L(\mathrm{H}) , \tag{4.1}$$

where we have assumed the number density of CO is $8.5 \times 10^{-5} n_{\rm tot}$ (this number is uncertain). $L(\mathrm{CO})$ is given by equation (6.23) of HM where the parameters are given in Table 3 of HM. Thus

$$L(\mathrm{CO}) = \frac{4(kT)^2 \times 9.7 \times 10^{-8}}{2.76 n_{\rm tot} k[1 + N_{\rm rat} + 1.5\sqrt{N_{\rm rat}}]} , \tag{4.2}$$

where

$$N_{\rm rat} = (3.3 \times 10^6 T_3^{1/2})/n_{\rm tot} \tag{4.3}$$

and $T_3 = T/1000$. For $T < 5$ K we set $L(\mathrm{CO})$ to zero. Contributions from $L(\mathrm{H})$ and $L(\mathrm{H}_2)$ can be obtained from equation (6.36) of HM. For example,

$$L(\mathrm{H}) = \frac{L_r(\mathrm{H})}{1 + [n_{\rm cr}^{\rm H}(\mathrm{rot})/n(\mathrm{H})]} + \frac{L_v(\mathrm{H})}{1 + [n_{\rm cr}^{\rm H}(\mathrm{vib})/n(\mathrm{H})]} , \tag{4.4}$$

and $L_r(\mathrm{H})$ and $L_v(\mathrm{H})$ are given by equations (6.37) and (6.38) of HM. These and other expressions contain many exponentials which are costly to compute. We therefore constructed tables of the subsidiary functions of T and used interpolation to save time. The terms in the denominators of equation (4.4) are given by equations (6.39), (6.40), and (6.41) of HM. As an example

$$\frac{n_{\rm cr}^{\rm H}(\mathrm{rot})}{n(\mathrm{H})} = \frac{L_r(\mathrm{H})}{L_r(\mathrm{H}, n \to 0)} , \tag{4.5}$$

where

$$L_r(\mathrm{H}) = \frac{1}{n(\mathrm{H})} \left\{ \left(\frac{9.5 \times 10^{-22} T_3^{3.76}}{1 + 0.12 T_3^{2.1}} \right) \exp\left[-\left(\frac{0.13}{T_3} \right)^2 \right] + 3 \times 10^{-24} \exp\left(\frac{-0.51}{T_3} \right) \right\} , \tag{4.6}$$

$$L_r(\mathrm{H}, n \to 0) = 0.25[5\gamma_2^{\rm H} e^{-(E_2 - E_0)/kT}(E_2 - E_0)] + 0.75[\tfrac{7}{3}\gamma_3^{\rm H} e^{-(E_3 - E_1)/kT}(E_3 - E_1)] , \tag{4.7}$$

and from equation (6.31)

$$\gamma_J^{\rm H} = \left(\frac{1 \times 10^{-11} T_3^{1/2}}{1 + 60/T_3^4} + 10^{-12} T_3 \right) [0.33 + 0.9 e^{-(J - 3.5/0.9)^2}] . \tag{4.8}$$

The energy levels (in ergs) in equation (4.7) are

$$E_0 = 0 , \quad E_1 = 1.185 \times 10^{-14} , \quad E_2 = 6E_1 , \quad E_3 = 12E_1 . \tag{4.9}$$

The equation for L_v analogous to equation (4.7) above requires the energies

$$E_{10} = 5860k , \quad E_{20} = 2E_{10} , \tag{4.10}$$

and the γ's that are given in equation (6.29) of HM. As noted above, the various γ's, the density-independent factor $L_r(\mathrm{H})$, and terms such as equation (4.7) can be calculated by interpolation in previously computed tables.

5. TIME STEPPING

The time stepping for the momentum equation and the particle shift equation is the predictor-corrector scheme (Anzer, Börner, & Monaghan 1987) which conserves linear and angular momentum when the gravitational force is calculated by direct summation. Because we use a grid there is a small error in the momentum conservation (<0.1%) and a small error in the angular momentum conservation (<0.01%) after 200 time steps. Because of the cooling it is necessary to use an implicit scheme for the energy equation (Monaghan & Varnas 1988; Hernquist & Katz 1989). Writing the energy equation for particle i in the form

$$f(T_i^1) = u_i(T_i^1) - u(T_i^0) - \delta t Q_i^{1/2} + \delta t \frac{\Lambda(T_i^1, n_i^{1/2})}{\rho_i^{1/2}} = 0 , \tag{5.1}$$

where $Q_i = -(P\nabla \cdot v/\rho)_i$ plus viscous dissipation (the summation term in eq. [2.7] is the SPH equivalent) and superscripts 0, $\frac{1}{2}$, 1 denote the beginning, midpoint, and final values for the time step. Equation (5.1) is a nonlinear equation for T_i^1. The Newton scheme is inappropriate to solve (5.1) because Λ is discontinuous (it is set to zero for $T \leq 5$ K and some terms are set to zero for $T < 50$ K). In any case, Λ is so complicated it is an advantage to avoid calculating derivatives. The procedure we used is a combination of bisection and the secant method. The initial guess for T_i^1 is T_i^0. If $f(T_i^1) > 0$ we halve the guessed value until we find a T_i^1 which gives f with the opposite sign. If $f(T_i^1) < 0$ initially we double T_i^1. This works because Λ increases with T. In this way we get two values of T_i^1 which straddle the correct value. Our root calculation then starts with one bisection step followed by cycles each of which consist of two secant steps and one bisection. The bisection step prevents convergence by the secant method from slowing down badly. We found that it was more efficient to use a fixed cycle rather than test to decide whether to have more secant or bisection steps. The stopping procedure was that

$$\left| \frac{f(T_i^1)}{u_i(T_i^0) + \delta t Q_i^{1/2}} \right| < 0.001 \quad \text{or} \quad \Delta T < \max\left(0.1, \frac{T_i^0}{1000} \right) , \tag{5.2}$$

where ΔT is the change in T_i^1 during the iteration. The second test was needed because f is discontinuous. About four or five evaluations of f were needed for convergence. Where the midpoint energy is required we use the approximation $0.5[u_i(T_i^1) + u_i(T_i^0)]$.

6. GRAVITATIONAL FIELD CALCULATION

To find the gravitational force on the particles their mass is assigned to a grid and Poisson's equation is represented on the grid by finite differences and solved by iteration. Forces are then calculated on the grid and assigned to the particles. We use a fourth-order scheme and iterate using a multigrid algorithm (Monaghan 1985; Monaghan & Varnas 1988). This solution requires that the surface potential is known. In previous work the surface potential was calculated by using the multi-

pole moments of the particles, a valid procedure because the grid formed a cubical box. In the present calculations we want sufficient resolution to study disk structures and this cannot be achieved if cells are wasted in a largely empty cubic box. A more efficient procedure is to use a rectangular grid that fits snugly around the matter, but this rules out finding the surface potential by multipole moments. For the disk system, expressions exist for the potential away from the matter, but they involve disproportionate amounts of computation. The procedure we finally adopted exploits the flexibility of the multigrid method.

A coarse grid (cell length scale twice that of the grid we eventually use) in the form of a cubical box was placed symmetrically around the matter. The mass of the particles was assigned to the vertices of this grid, using a resolution length appropriate to the scale of the box, and the surface potential calculated by multiple moments and the solution found by multi-grid iteration (Monaghan & Lattanzio 1985).

The solution on the coarse grid is then interpolated to the vertices of a fine grid which forms a rectangular box fitting snugly around the matter. The values of the potential on the coarse cubical grid, where they match the fine rectangular grid, provide both the surface potential and starting values for a new multigrid iteration based on the fine grid.

On a Vax 11/780 or Vax 8700 we typically use a maximum of 80,000 cells. For a cubical array this implies ~ 43 cells in a coordinate direction. Because the method is fourth order the multigrid cell width can go up to $2h$ (h is the length used in W_{ij}) while still providing accuracy comparable to the SPH part of the calculation. The equivalent grid, if the typical second-order finite difference scheme is used, is therefore at least $(86h)^3$.

We allow for a minimum number of vertices in any direction of 17. For a disk configuration this leaves ~ 4700 vertices for the plane of the disk and typically 68 vertices across a diameter. The equivalent for a second-order scheme is at least 136 vertices across a diameter and a total of $34 \times 136 \times 136 = 630{,}000$ cells.

We have also introduced some technical refinements. The algorithm now uses four grids (others may be added easily) each of which uses a cell width twice that of the next finest. The coarsest grid therefore has 1/512 of the cells on the fine grid. A typical solution by iteration takes work equivalent to about eight sweeps on the finest grid.

The iteration is stopped when the maximum change of the potential on the fine grid is $< 10^{-5}(4\pi G\rho H^2)$, where H is the cell width. Coarser grids use a similar rule with $4\pi G\rho H^2$ replaced by the appropriate source term.

The algorithm has been tested by using analytical density distributions with known potentials, by calculating the forces on small sets of particles and by following binary systems. A binary system serves as a severe test, since it involves a sharply varying density and the assignment to and from the grid. The computed force has typical errors relative to the exact value of 2×10^{-5}.

7. INITIAL STATES AND STABILITY

In this paper we follow the evolution of gas clouds and disk systems. The clouds are initially spherical with mass $M = 10^4$ $M_\odot$ and radius $R = 12.6$ pc. For some of the sequences the initial density is uniform. In others the density is given a random perturbation. For most of the cloud calculations the initial temperature is 70 K, although we ran three sequences at 65, 117, and 184 K to sample the three regions delineated by Miyama, Hayashi, & Narita (1984, hereafter MHN). We discuss this further below.

The disk system we evolve is a perturbed Maclaurin disk with radius R, constant angular velocity and surface density $\propto (1 - r^2/R^2)^{1/2}$.

It is useful to recall what theory tells us about the isothermal collapse. From Larson's (1985) review and discussion of fragmentation, the critical wavelength λ_c for fragmentation from a uniform medium of density ρ is

$$\lambda_c = \left(\frac{\pi\gamma c^2}{G\rho}\right)^{1/2}, \tag{7.1}$$

where c is the isothermal sound speed and γ is the adiabatic index. The critical mass M_c given by Larson (1985) is

$$M_c = 8.53\left(\frac{\gamma c^2}{G\rho}\right)^{3/2}\rho\,. \tag{7.2}$$

During isothermal collapse both λ_c and M_c decrease. This is the basic idea behind Hoyle's (1953) theory of fragmentation which predicts that, as M_c is reduced, smaller fragments will separate from the collapsing cloud. In practice, this does not occur because the fragments do not have time to separate out in a purely spherical collapse.

For an initial spherical cloud with constant density, mass M, and radius R it is convenient to write

$$\lambda_c = 3.63R\sqrt{\gamma\zeta}\,, \quad M_c = 17.45(\gamma\zeta)^{3/2}M\,, \tag{7.3}$$

where

$$\zeta = \frac{TR\,\mathfrak{R}_0}{GM\mu} = 0.0019\,\frac{T}{\mu}\left(\frac{R/\mathrm{pc}}{M/1000\ M_\odot}\right). \tag{7.4}$$

The ratio of thermal to gravitational energy is

$$\alpha = \frac{5\zeta}{3(\gamma - 1)}\,, \tag{7.5}$$

where the adiabatic index γ is ~ 1.4 for $T < 80$ K. The ratio of rotational energy to gravitational energy, when the angular velocity is constant, is

$$\beta = \frac{1}{3}\,\frac{Rv_e^2}{GM} = 0.077\left(\frac{R/\mathrm{pc}}{M/1000\ M_\odot}\right)\left(\frac{v_e}{\mathrm{km\ s^{-1}}}\right)^2, \tag{7.6}$$

where v_e is the equatorial velocity.

The regions delineated by MHN are (1) $\alpha\beta > 0.2$ which can form an equilibrium cloud if there is an external pressure; (2) $0.12 < \alpha\beta < 0.2$ when contraction occurs to a nonfragmentating disk system; and (3) $\alpha\beta < 0.12$ which produces a fragmenting disk. By taking $v_e = 1.7$ km s^{-1} and $T = 65$, 116, and 184 K we sample each of these $\alpha\beta$ regions if the gas is isothermal. The results of an isothermal evolution of these sequences (see § 10.2) generally confirm the results of MHN.

For a sequence starting with $T = 70$ K, standard M (i.e., 10^4 $M_\odot$, as quoted above) and R (12.6 pc), $\mu = 2.33$, and $v_e = 2.2$ km s^{-1}, the stability parameters are $\zeta = 0.073$, $M/M_c = 0.74$, $\alpha = 0.30$, $\beta = 0.47$, and $\alpha\beta = 0.141$. We therefore expect the cloud to collapse and form a nonfragmenting disk if T is constant. This evolution is discussed in §§ 10.3 and 10.4.

The ultimate fate of any isothermal cloud depends crucially on the rotation and this is incorporated in the criterion of MHN. An alternative description of fragmentation of any disk

state that occurs is given by Toomre's (1964) estimate of the relative effects of rotation, pressure (or velocity dispersion), and self-gravity.

For a nonrotating infinitely thin disk the critical mass (see Larson 1985) is

$$M_c = 1.17 \frac{\gamma^2 c^4}{G^2 \sigma}, \tag{7.7}$$

where σ is the mass per unit area. For a rapidly rotating cloud we estimate σ by $M/(\pi R^2)$ where R is the initial cloud radius. In this case

$$\frac{M_c}{M} = 1.17\pi\gamma^2\zeta^2 = 0.02, \tag{7.8}$$

if $\zeta = 0.073$, which shows, as expected, that many more fragments can form in the disk configuration than form in the spherical distribution with the same M, R, and T (for which $M_c/M = 0.34$).

Rotation changes this picture. Larson (1985) proposed, in agreement with Toomre, that the stability indicator is

$$Q = \frac{\kappa c}{\pi G \sigma}, \tag{7.9}$$

where c is the isothermal sound speed and κ the epicyclic frequency, defined by

$$\kappa^2 = 2\Omega\left(\varpi \frac{d\Omega}{d\varpi} + 2\Omega\right), \tag{7.10}$$

where ϖ is the radial coordinate in the disk. The instability indicator is $Q < Q_c$ where Larson (1985) estimates (using results from Goldreich & Lynden-Bell 1965) that $Q_c \sim 0.55$. An alternative argument by Hachisu, Tohline, & Eriguchi (1987) is based on the idea that fragmentation will occur in a disk if two conditions are met. These are that the ratio of the gravitational free-fall time $t_{\rm ff}$ to $t_s = 2\pi\varpi/c$ is sufficiently small, and the ratio of $t_{\rm ff}$ to the epicyclic period $t_{\rm ep}$ is also sufficiently small. With suitable averaging Hachisu et al. (1987) show that $(t_{\rm ff}/t_s)$ $(t_{\rm ff}/t_{\rm ep}) \propto Q$.

For the Maclaurin disk

$$\sigma = \frac{3M}{2\pi R^2}\left(1 - \frac{r^2}{R^2}\right)^{1/2}, \quad \Omega = \left[\frac{3G\pi M}{(4R^3)}\right]^{1/2} \tag{7.11}$$

so that

$$Q \sim \frac{2\zeta^{1/2}}{[1 - (r^2/R^2)]^{1/2}}. \tag{7.12}$$

For a disk with $T = 70$ K, $M = 10^4\ M_\odot$, $R = 12.6$ pc, $\zeta = 0.073$ so that $Q \sim 0.54/(1 - r^2/R^2)^{1/2}$. We therefore expect the isothermal disk to be just unstable in the central regions and stable in the outer regions. With molecular cooling the disk temperature can drop to 5 K, so that $Q \ll Q_c$ and fragmentation is expected over most of the disk.

In practice none of the instability indicators are entirely satisfactory because the collapsing cloud does not necessarily pass through near-equilibrium states.

We may estimate the cooling time scale $\tau_{\rm cool}$ from CO molecules (the dominant source) quite simply. Consider one of our standard clouds composed of pure hydrogen, except for trace amounts of CO in ratio $n({\rm CO})/n_{\rm tot} = 8.5 \times 10^{-5}$. Then

$$\tau_{\rm cool} \simeq \frac{\rho u}{\Lambda} = m_{\rm H} n_{\rm tot}\left(\frac{1.5kT}{m_{\rm H}}\right)\left[\frac{1}{n_{\rm tot}^2 L({\rm CO}) 8.5 \times 10^{-5}}\right].$$

Using equation (4.2) we get

$$\tau_{\rm cool} \simeq \frac{1.2 \times 10^{11}}{T}(1 + N_{\rm rat} + 1.5\sqrt{N_{\rm rat}})$$

where $N_{\rm rat} = [3.3 \times 10^6 (T/1000)^{1/2}]/n_{\rm tot} \simeq 1.7 \times 10^4$ initially. So the initial cooling time is

$$\tau_{\rm cool} \simeq 10^6 \text{ yr}.$$

This is to be compared with the initial free-fall time-scale

$$t_{\rm ff} = \left(\frac{3\pi}{32G\rho}\right)^{1/2} \simeq 7.4 \times 10^6 \text{ yr},$$

and the rotation period of

$$P = \frac{2\pi R}{v_e} \simeq 3.5 \times 10^7 \text{ yr}.$$

Thus we expect the cooling to have significant effects on the dynamics.

8. PARTICLE CONFIGURATION

For the uniform spherical clouds the (equal mass) particles are arranged on a lattice and those within R of the origin are retained. In the past we have used a lattice with cubical cells, but in the present calculation we use a body-centered cubic lattice. The reasons for doing this are that it is equivalent to the centroid method of numerical integration (Good & Gaskins 1971), and that it is the best distribution for transmitting information from a continuum set of data (Sloane 1986; the two-dimensional equivalent, hexagonal cells, shows up naturally in two-dimensional particle schemes, e.g., Daly, Harlow, & Welch 1964, p. 47).

The randomly perturbed uniform sphere is produced by choosing three random numbers q_1, q_2, and q_3 in $0 < q_i < 1$, then calculating the spherical polar coordinates r, θ, and ϕ according to

$$r = Rq_1^{1/3}, \quad \cos\theta = 2q_2 - 1, \quad \phi = 2\pi q_3. \tag{8.1}$$

For the Maclaurin disk the particles, again each of equal mass, are positioned randomly within a circle of radius R in such a way that the average density is $\propto (1 - r^2/R^2)^{1/2}$. We did this in two ways. In the first two random numbers q_1 and q_2 in $0 < q_i < 1$ were calculated and the plane polar coordinates determined by

$$r = R(1 - q_1^{2/3})^{1/2}, \quad \phi = 2\pi q_2. \tag{8.2}$$

A random configuration in the Maclaurin disk can also be produced by the rejection technique (e.g., Hohl & Hockney 1969). In this case sets of three random, numbers q_1, q_2, and q_3 in $0 < q_i < 1$ are generated and accepted if

$$q_1^2 + q_2^2 \le 1, \quad q_3 \le \sqrt{(1 - q_1^2 - q_2^2)}. \tag{8.3}$$

If they are accepted then the particle is given the Cartesian co-ordinates

$$x = 2q_1 - 1, \quad y = 2q_2 - 1, \quad z = 0. \tag{8.4}$$

The two methods give different perturbations and different fragments.

9. SCALING

The unit of mass is M, the total mass of the cloud or disk. The unit of length is R, the initial radius of the cloud or disk.

The unit of energy is then GM/R and the unit of density is M/R^3. The unit of time τ is $(R^3/GM)^{1/2}$ so that the free-fall time is 1.1τ. To allow easy conversion of computed values into cgs units we provide the following conversion formulae:

$$\text{with } R^* = R/(5\text{ pc}), \quad M^* = M/(1000\ M_\odot)$$

then

$$\tau = 1.658 \times 10^{14}(R^{*3}/M^*)^{1/2}\text{ s},$$

$$\text{velocity} = 9.303 \times 10^4(M^*/R^*)^{1/2}\text{ cm s}^{-1},$$

$$\text{density} = 0.544 \times 10^{-21}(M^*/R^{*3})\text{ g cm}^{-3},$$

$$\text{energy} = 8.652 \times 10^9(M^*/R^*)\text{ ergs}. \quad (9.1)$$

The scaled pressure P is given by

$$P = \frac{\rho T}{\mu}\left(\frac{R\Re_0}{GM}\right) \quad (9.2)$$

where ρ is the scaled density.

10. THE SIMULATIONS

10.1. *Maclaurin Disks*

We begin with the Maclaurin disk (see § 7) because it provides a convenient test of the ability of our algorithm to handle disk systems, and shows clearly how cooling affects the evolution.

Our disk has a mass of $10^4\ M_\odot$ and radius $R = 12.6$ pc. The initial temperature was $T = 70$ K and we used both 4000 and 32,000 particles. The equilibrium Maclaurin disk has a surface density $3M(1 - r^2/R^2)^{1/2}/(2\pi R^2)$ and constant angular velocity $\Omega = [3G\pi M/(4R^3)]^{1/2}$. The Q factor for stability is (see eqs. [7.8] and [7.9]):

$$Q \sim \frac{2\zeta^{1/2}}{(1 - r^2/R^2)^{1/2}} \sim \frac{0.54}{(1 - r^2/R^2)^{1/2}} \quad (10.1)$$

so that, if the disk remains isothermal, we can expect some fragmentation in the central regions, but the other regions should remain stable. When molecular cooling occurs, most of the disk should fragment. In our units the equilibrium $\Omega = [(3\pi/4)]^{1/2} = 1.53$.

Figure 1 shows the development of fragments in a disk with molecular cooling and $N = 32{,}000$. The fragmentation is extremely rapid and occurs over most of the disk. The overall appearance is that of clumps connected by filaments with many voids. The filaments appear to be the natural response of the rotating disk to clump formation (Julian & Toomre 1966).

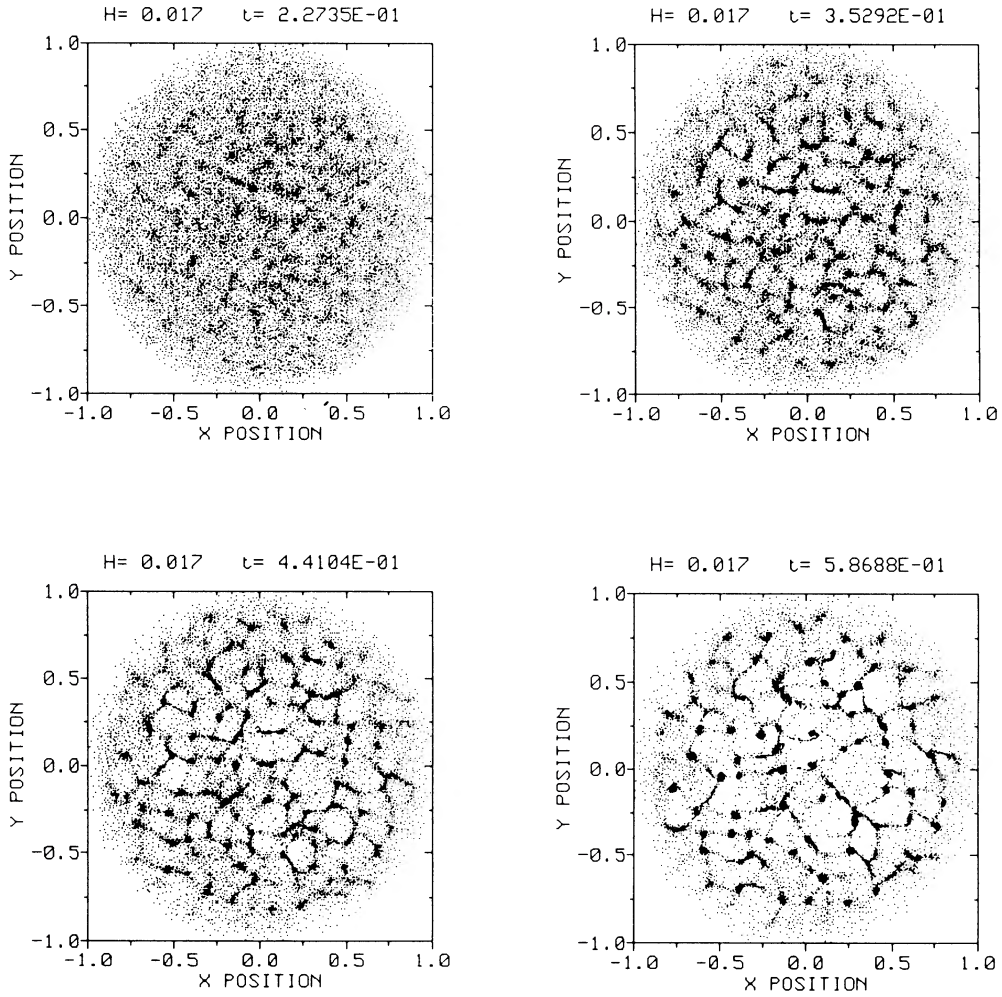

FIG. 1.—A Maclaurin disk with molecular cooling. The resolution length is H, and the time is given in units of $\tau = (R^3/GM)^{1/2}$.

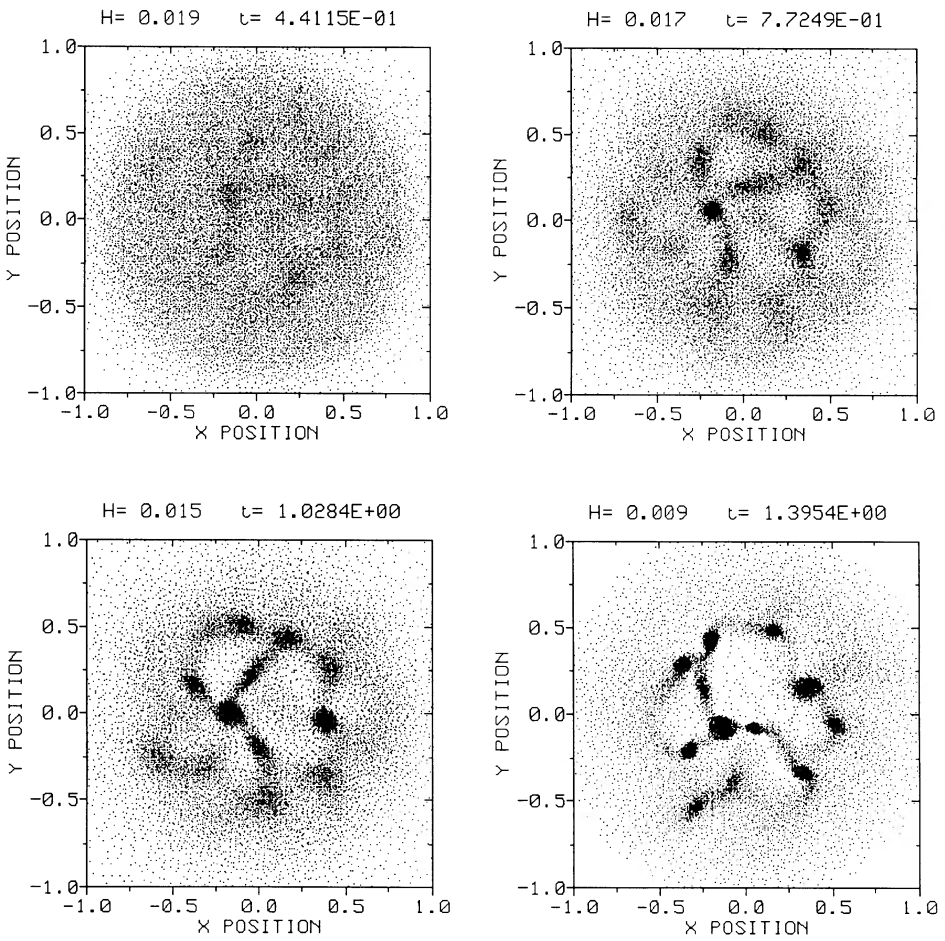

FIG. 2.—Same as Fig. 1, but for the isothermal equation of state

If the gas is kept at 70 K then equation (10.1) predicts that the central regions may just be unstable to fragmentation but the outer regions will remain stable. Figure 2 shows an isothermal evolution (with $N = 32{,}000$) with the same field of random perturbations that produced Figure 1. (Similar results were seen with $N = 4000$, in contrast to the cooling sequence.) It is clear that fewer and weaker fragments occur, and they are closer toward the center than was the case for the cooling sequence. The isothermal sequence produces maximum densities which are lower than the cooling sequence at equivalent times. Indeed, the time scale for the collapse in the cooling sequence is lower by a factor ~ 3. Figure 3 shows that roughly equivalent densities are reached 3 times later in the isothermal sequence.

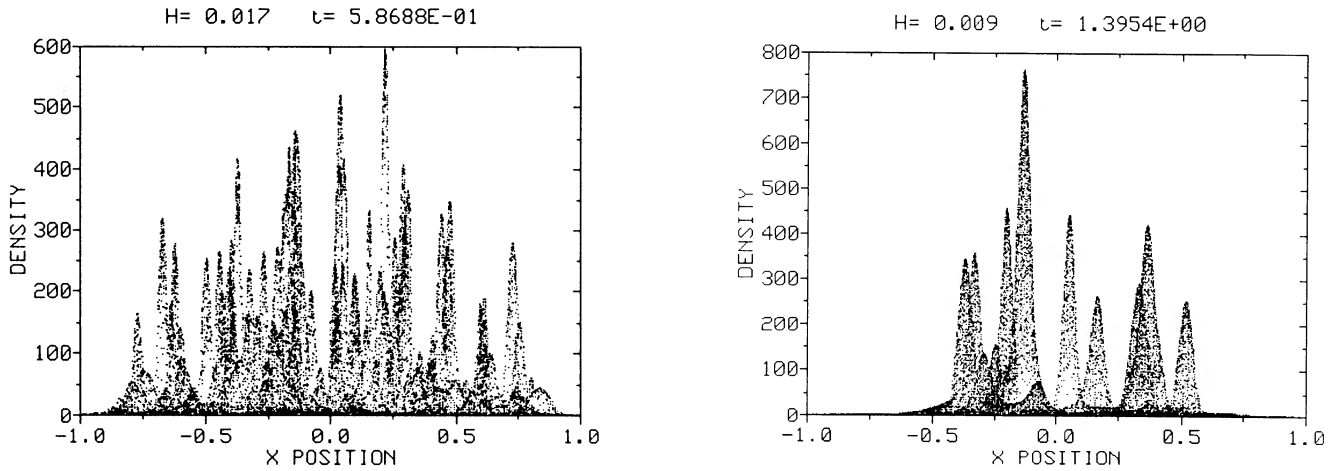

FIG. 3.—Densities for the cooling disk (*left*) and isothermal disk (*right*) at the quoted times.

That the cooling sequence results in more fragments is expected since the length scale of maximum growth

$$H = \frac{c^2}{\pi G \sigma}$$

is proportional to the temperature. Thus the fragments seen in Figure 2 are expected to be of a scale ~ 14 times the fragments seen in Figure 1, which is roughly what is found. However, the Fragments in Figure 1 are not described accurately because their scale is comparable to the resolution length h.

When the perturbations are set up by the rejection method the fragments are fewer in number and the filaments are longer. These results are similar to those found by Hohl & Hockney (1969). In their calculation, however, the particles simulated a collisionless system, whereas in our simulation the particles represent a noninterpenetrating gas. For cold disks with 50,000 particles and a 64 × 64 grid their calculation produces more filaments in the outer parts of the disk. These differences are probably due to the fact that the outer parts of our disk are stable. When Hockney & Hohl introduce velocity dispersion the number of filaments and fragments reduces as the dispersion increases.

10.2. *Isothermal Sequences with $\alpha\beta = 0.047, 0.14, 0.21$*

These sequences were run to compare with the calculations of MHN. They differ from those calculations in three ways: we use more particles (6912 compared to 4000), we do not include a surface pressure, and we use a resolution length h which is fixed in space (but varies with time). This fixed h is adequate to resolve the ring-mode instability which develops, but it is not able to resolve structures an order of magnitude smaller.

All sequences have $M = 10^4\ M_\odot$ and start with a spherical cloud of radius $R = 12.6$ pc. The particles are placed randomly according to the procedure described in § 8. The equatorial velocity is 1.7 km s^{-1}, so that initially $\beta = 0.28$. The temperature for the three sequences are 65, 117, and 184 K.

The sequence with initial $\alpha\beta = 0.047$ is expected to fragment. In Figure 4 we show the particle positions projected on to the $x - y$ and $x - z$ planes at $t = 1.92 = 2.1 t_{\rm ff}$. The disk is highly flattened, and a nonaxisymmetric dense inner disk is forming. The inner region becomes unstable as indicated by the density plot of Figure 5, and the velocity and particle position plots of Figure 6. Figure 6 suggests the ring mode instability predicted by Goldreich & Lynden-Bell (1965) although their analysis assumes uniform rotation which is only a crude approximation to the actual rotation seen in the disk prior to ring formation. They also assume an external pressure, but this can be taken to be small and should not have a strong effect on the dynamics. The ring mode has a maximum instability for a wavelength $\lambda_c \simeq 2\pi z_d$, where z_d is the half-thickness of the disk. we find $z_d \sim 0.05$ and estimate $\lambda_c \sim 0.3$ which is in satisfactory agreement with our results.

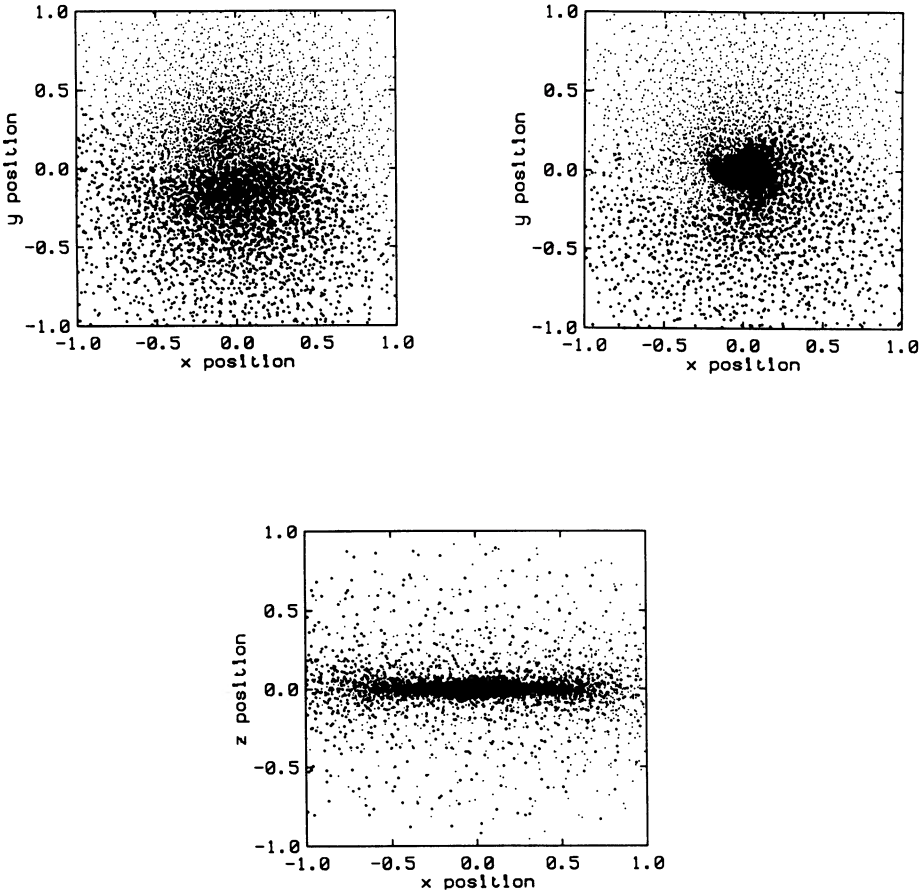

FIG. 4.—Evolution of isothermal spheres of initial $\alpha\beta = 0.047$. The upper figures are at $\tau = 1.55$ (*left*) and 1.92 (*right*). The lower figure is an x-z projection for $\tau = 1.55$.

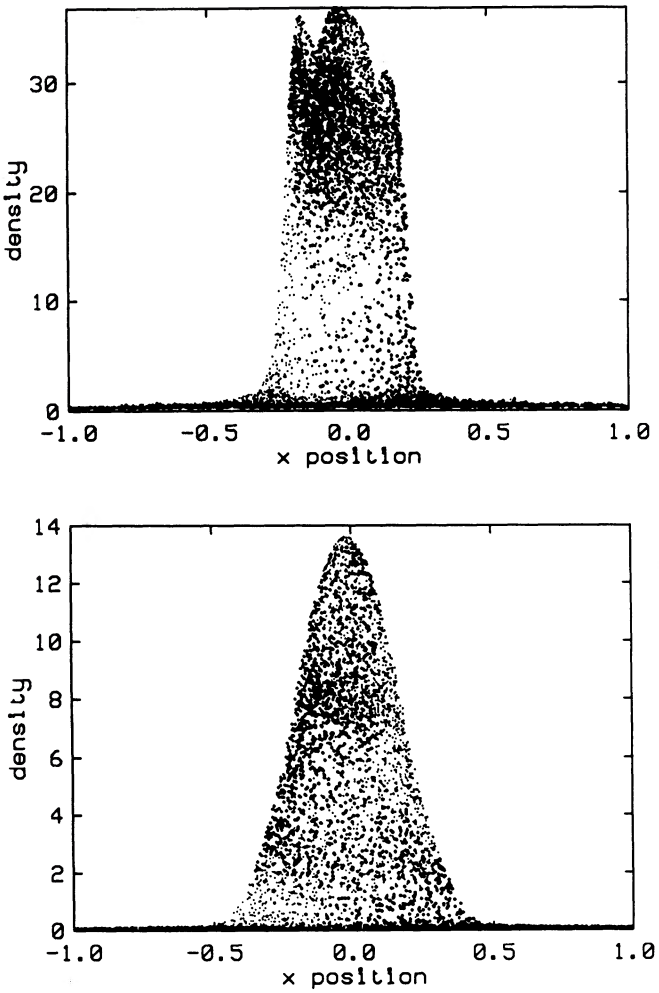

FIG. 5.—Density plots for the isothermal spheres with $\alpha\beta = 0.047$ at $\tau = 2.16$ (*upper*) and $\alpha\beta = 0.14$ at $\tau = 3.04$ (*lower*).

These results are in general agreement with MHN, but they find fragmentation into clumps occurs earlier than our calculations predict. These differences are not due to the better resolution provided by the spatially variable resolution used by MHN, because we have adequate resolution to see the clump formation. We are currently exploring the possibility

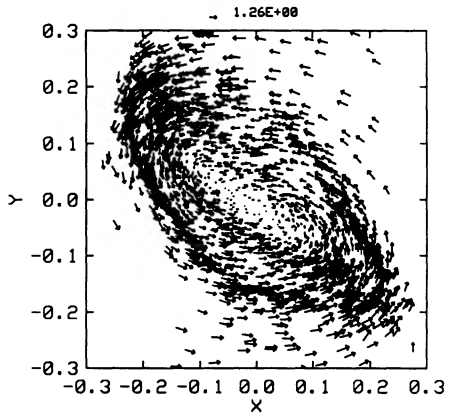

FIG. 6.—Velocity in the x-y plane for the $\alpha\beta = 0.047$ case at $\tau = 2.66$. Only particles near the origin are shown.

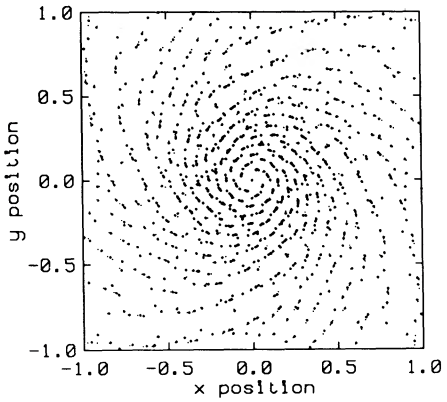

FIG. 7.—Particle positions in the x-y plane at $\tau = 3.44$ for the smooth isothermal sphere.

that the differences are due to the different artificial viscosities used. It is already clear from other calculations (Gingold & Monaghan 1983) that the spiral clumps found by MHN occur when the artificial viscosity is large, and MHN state that the nonaxisymmetric perturbation grows during the "ϖ-bounce," when the viscosity is at its largest. Also, the solid-body rotation

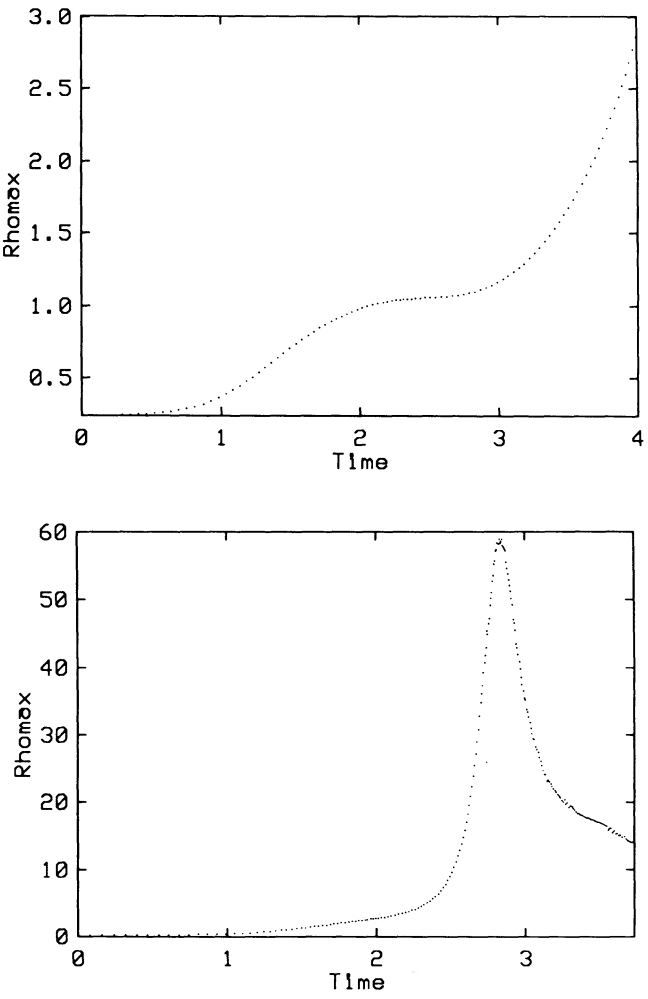

FIG. 8.—Run of maximum density with time (in τ) for the smooth isothermal sphere (*upper*) and cooling sphere (*lower*).

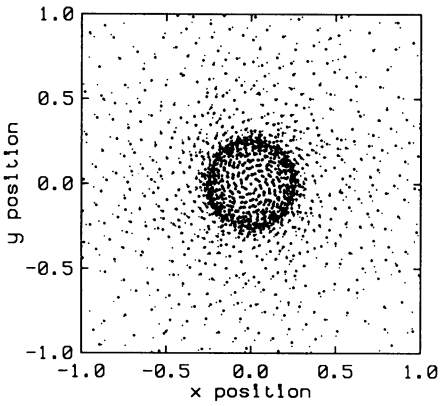

FIG. 9.—Particle positions in the x-y plane at $\tau = 3.13$ for the smooth cooling sphere.

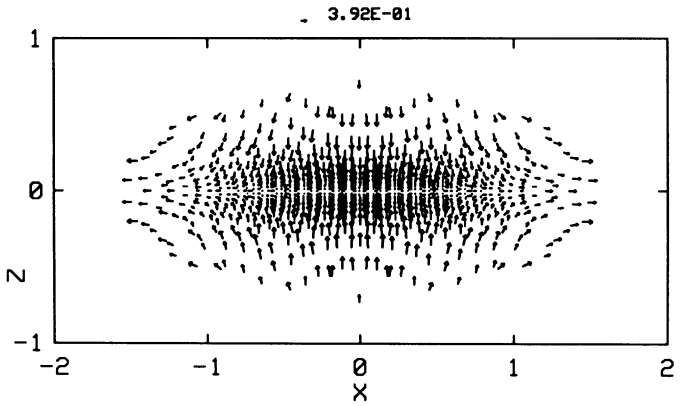

FIG. 11.—Velocity field in the x-z plane through the rotation axis of the smooth cooling sphere at $\tau = 1.24$.

seen in their fragments may be another indication that the viscosity is large (see Lattanzio & Henriksen 1988). Certainly the fragmentation observed in this paper is qualitatively different. MHN find that a spiral forms and then fragments, whereas in our calculations the fragmentation occurs first.

The sequence with $\alpha\beta = 0.14$ behaves similarly to those described by MHN. A disk forms, but it is much thicker than the previous disk. No ring forms.

The sequence with $\alpha\beta = 0.21$ continually expanded during the time we followed it. If we had included an external pressure we would have expected this cloud to reach an equilibrium, in agreement with the results of MHN.

Taken together, the results for these sequences and for the Maclaurin disks show that our calculations give results in agreement with theory (Hachisu & Eriguchi 1985; Stahler 1983; Larson 1985) and other numerical experiments (MHN). In the following sections we describe the evolution of a standard cloud under different conditions.

10.3. *A Smooth Spherical Cloud*

Our standard cloud has $M = 10^4\ M_\odot$, $R = 12.6$ pc, $T = 70$ K, and $v_e = 2.2$ km s^{-1}: thus initially $\alpha = 0.30$, $\beta = 0.47$, and $\alpha\beta = 0.141$. The rather high value of v_e and therefore β was chosen to ensure that, for temperatures appropriate to molecular clouds, the initial $\alpha\beta \sim 0.15$ and we should not expect the isothermal sequence to fragment. Since we expect a cooling sequence to be more unstable and to fragment, the differences are highlighted. The cloud was started in the smooth state (particles on a body-centered lattice) with 12,912 particles and two sequences were run: one isothermal and one with molecu-

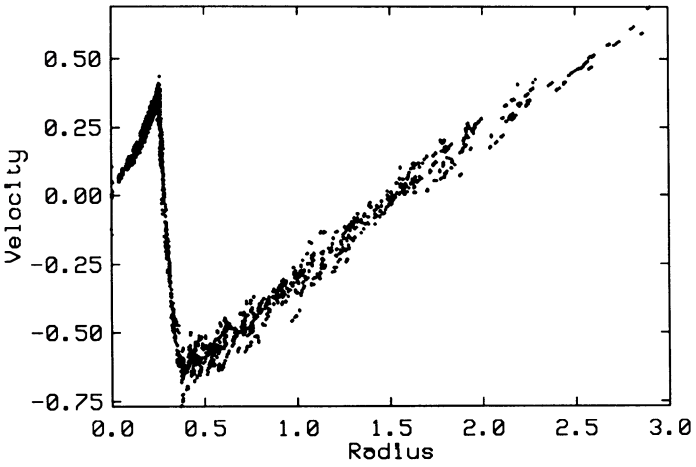

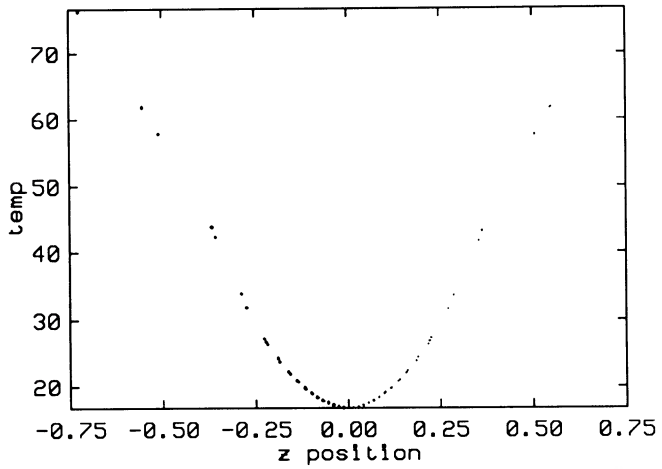

FIG. 10.—Temperature vs. vertical height (z) for the smooth cooling sphere at $\tau = 1.24$.

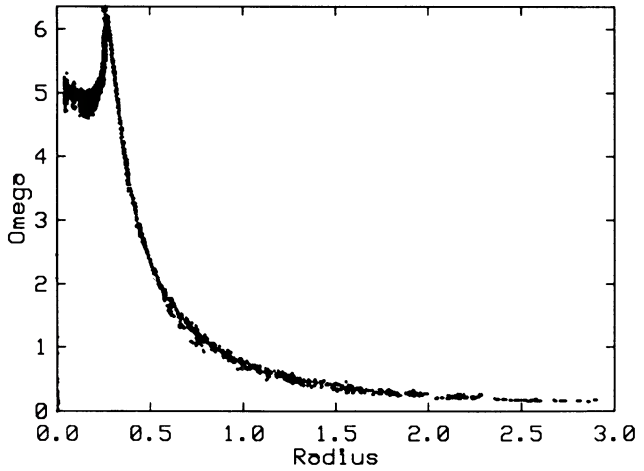

FIG. 12.—Radial velocity (*upper*) and rotational frequency (*lower*) vs. radius for the smooth cooling sphere at $\tau = 3.13$.

lar cooling. From the results described in § 10.2 we expect the isothermal cloud to collapse to form a disk which does not fragment. The molecular cooling causes the cloud to rapidly pass through states which can only be reached, if at all, by isothermal clouds at much lower temperature.

In Figure 7 we show the particle positions from the isothermal sequence, projected onto the x-y plane. Although the effect of the initial lattice structure is clearly seen, there is no fragmentation. At this stage the cloud has formed a differentially rotating disk with a half-thickness of 0.07. In Figure 8 we show the maximum density as a function of time.

The particle positions from the cooling sequence are shown projected onto the x-y plane in Figure 9 at $t \simeq 2.0t_{\rm ff}$. A ring has formed and, as before, we associated this with the ring-mode instability of Goldreich and Lynden-Bell. The time variation of the maximum density $\rho_{\rm max}$ is shown in Figure 8.

The strong effect of cooling is clear from Figure 10 which shows the run of temperature with z along the rotation axis. Figure 11 shows the velocity field in an $x - z$ slice through the center of the cloud. The shocks above and below the disk are evident.

In Figure 12 we show the radial velocity and angular veloc-

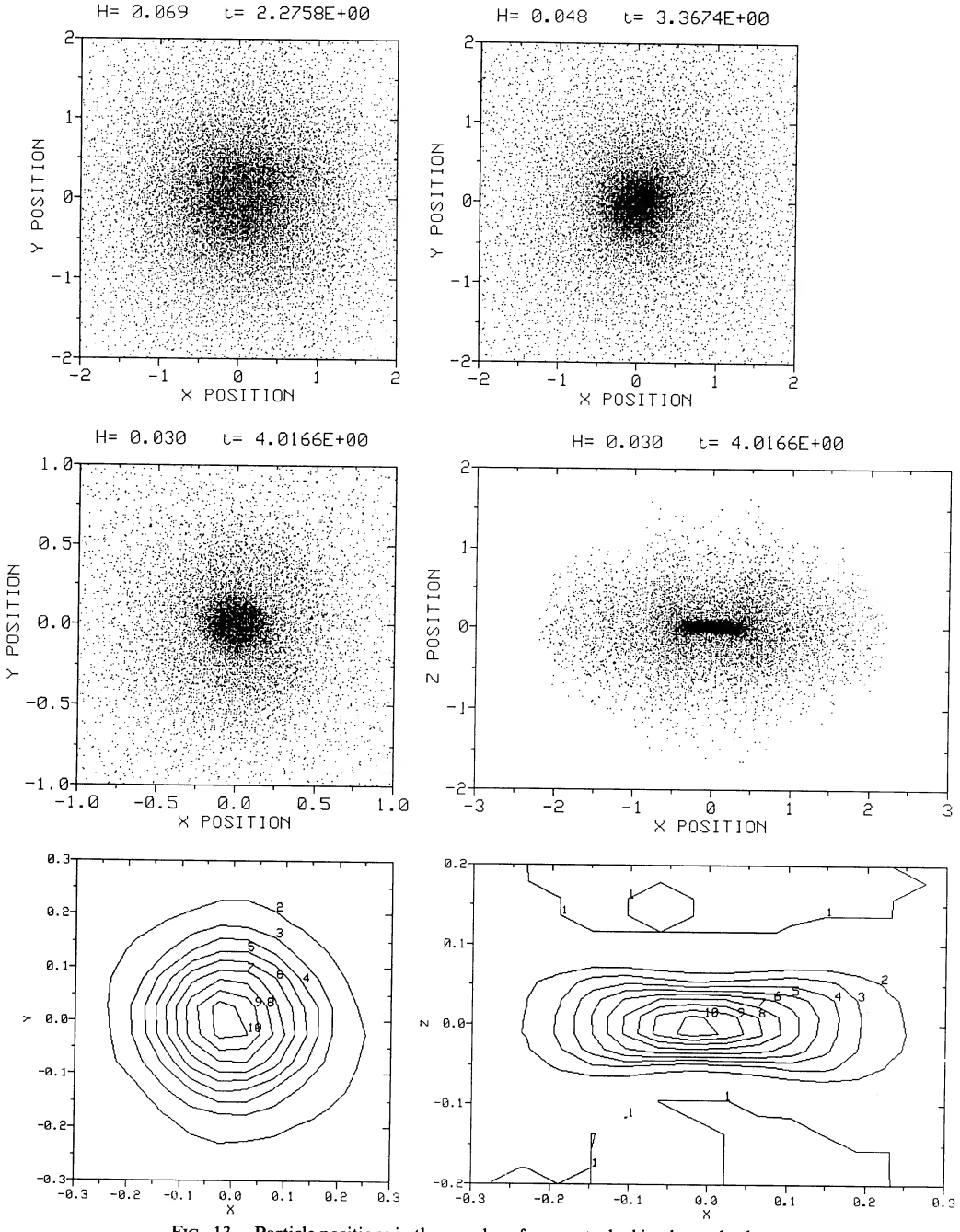

FIG. 13.—Particle positions in the x-y plane for a perturbed isothermal sphere

ity of the disk which forms from the cooling cloud. A small fraction of the matter beyond $r \simeq 1.5$ is expanding outward, and the bounce is clearly seen. The angular velocity Ω is given very roughly, by $\Omega \simeq 1/r$ for $r > 0.25$. This gives an azimuthal velocity variation with r similar to that observed for spiral galaxies.

The angular velocity z for the isothermal sequence shows more variation for a given r than is the case for the cooling sequence. The formula for Ω for the isothermal sequence is $\Omega \simeq 0.5/r$ for $r > 0.5$, but for $r < 0.5$ there is too much scatter and Ω cannot be considered, even approximately, as a function of r.

10.4. *A Perturbed Spherical Cloud*

In these sequences we take the same M, R, v_e, and initial T as before but choose the particle positions at random (see § 8).

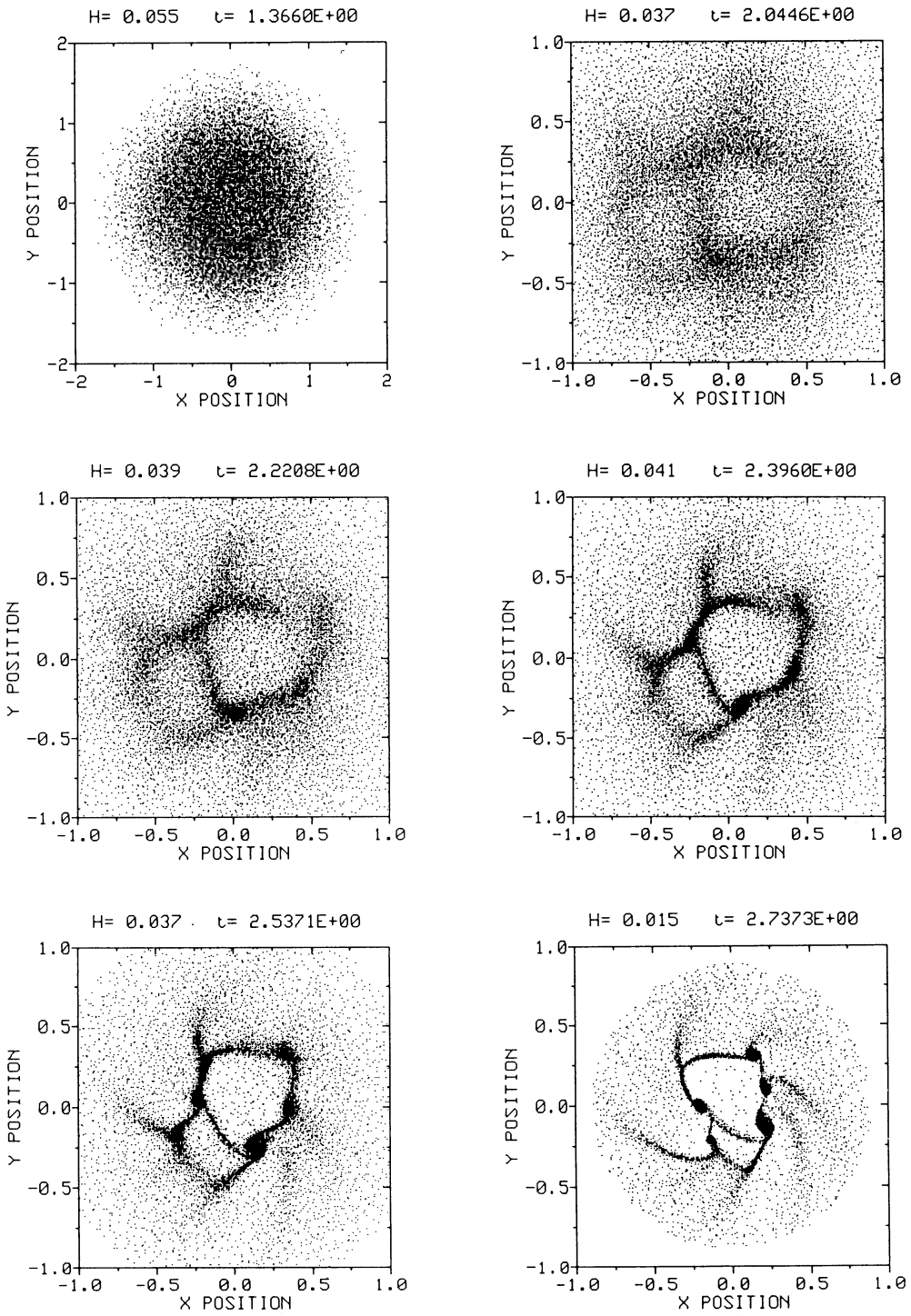

FIG. 14.—Same as Fig. 13, but for an isothermal equation of state evolutions

There is now an initial field of density perturbations with a standard deviation of 14%. The isothermal sequence forms a differentially rotating disk (see Fig. 13). The ratio of the final (calculated) maximum density (at $t \simeq 4t_{\rm ff}$) to the initial density ρ_0 is 40. This value is strongly dependent on the resolution because a small amount of matter at the center reaches the highest density, and the resolution is controlled by the bulk of the matter. Fragmentation does not occur.

The cooling sequence behaves quite differently. The development of a set of dense filaments is shown in Figure 14. Similar configurations of filaments and knots are seen in cosmological calculations, though here they arise from a collapsing differentially rotating cloud rather than in an expanding universe. At the time the calculations were stopped the filaments had not fragmented, but they can be expected to do so. By the time of the conclusion of calculations the temperature is ~ 5 K, and the ratio of the initial critical mass M_c (see eq. [7.2]) to the critical M_c at this stage is 1600. The maximum density rises from its initial value of $3/(4\pi)$ rather slowly at first. It increases rapidly at $t \simeq 2.5$, and by $t = 2.8$ the maximum density is ~ 2800 giving an increase by a factor of 10^4, due to the runaway collapse which has been initiated in the lumps.

The configuration shows a remarkable similarity to the star-forming region W49A (Welch et al. 1987). The knots in the ring are gravitationally unstable, and we would expect star formation to occur in these condensations. We identify these with the H II regions in W49A. Note that we form a ring quite naturally, with no need for a central mass. This complex will be the subject of a future investigation.

11. CONCLUSIONS

The results of the calculations show that the inclusion of molecular cooling is essential for the understanding of the fragmentation of rotating clouds. The cooling is so effective that the gas is typically cooled to 10 K in one-free-fall time. Pressure forces are then small by comparison with gravity, and the fluid behaves like an N-body system which, however, retains the essential fluid property of non-penetration of colliding streams.

The cooling clouds invariably collapse to differentially rotating disks. If the initial state is very smooth a ring-mode instability occurs. With random perturbations the instability is more complicated. The rotation law in the disk is similar to that for a galaxy.

We thank Rod Whitaker of Los Alamos National Laboratory for making available to us the routine he has used (Hunter et al. 1986) for flows with molecular cooling. Although we wrote our own routine for use on the Cray we are indebted to him for convincing us that it was easy to compute molecular cooling.

Work performed partly under the auspices of the US Department of Energy by the Lawrence Livermore National Laboratory under contract No. W-7405-ENG-48. Part of this work has been conducted under the auspices of a special NASA astrophysics theory program that supports a joint Center for Star Formation Studies at NSA-Ames Research Center, University of California, Berkeley, and University of California, Santa Cruz.

REFERENCES

Aller, L. H. 1964, The Atmospheres of the Sun and Stars (New York: Ronald Press), p. 119
Anzer, U., Börner, G., & Monaghan, J. J. 1987, A&A, 176, 235
Daly, B. J., Harlow, F. W., & Welch, J. E. 1964, Numerical Fluid Dynamics Using the Particle-and-Force Method, Los Alamos National Lab. Rept., LS-3144
Gingold, R. A., & Monaghan, J. J. 1983, MNRAS, 204, 715
Goldreich, P., & Lynden-Bell, D. 1965, MNRAS, 130, 125
Good, I. J., & Gaskins, R. A. 1971, Numer. Math., 16, 343
Hachisu, I., & Eriguchi, Y. 1985, A&A, 143, 355
Hachisu, I., Tohline, J. E., & Eriguchi, Y. 1987, ApJ, 323, 592
Hernquist, L., & Katz, N. 1989, ApJS, 70, 419
Hohl, F., & Hockney, R. 1969, J. Comput. Phys., 4, 306
Hollenbach, D. 1988, Ap. Letters Comm., 26, 191
Hollenbach, D., & McKee, C. 1979, ApJS, 41, 555
Hoyle, F. 1953, ApJ, 118, 513
Hunter, J. H., Sanford, M. T., Whitaker, R. W., & Klein, R. I. 1986, ApJ, 305, 309
Julian, W. H., & Toomre, A. 1966, ApJ, 146, 810
Larson, R. B. 1985, MNRAS, 214, 379
Lattanzio, J. C., & Henriksen, R. N. 1988, MNRAS, 232, 565
Miyama, S. M., Hayashi, C., & Narita, S. 1984, ApJ, 279, 621 (MHN)
Monaghan, J. J. 1985, Computer Phys. Rept., 3(2), 71
———. 1988, Computer Phys. Comm., 48, 89
Monaghan, J. J., & Lattanzio, J. C. 1985, Astr. Ap., 149, 135
Monaghan, J. J., & Varnas, S. 1988, MNRAS, 231, 515
Noh, W. 1987, J. Comput. Phys., 72, 78
Sloane, N. J. A. 1986, Notices American Math. Soc., 33, 40
Stahler, S. W. 1983, ApJ, 268, 165
Toomre, A. 1964, ApJ, 139, 1217
Welch, Wm. J., Dreher, J. W., Jackson, J. M., Tereby, S., & Vogel, S. N. 1987, Science, 238, 1550